Direct photon production from hadronic sources in high-energy heavy-ion collisions

E. L. Bratkovskaya,[1] S. M. Kiselev,[2] and G. B. Sharkov[2]
[1]*Frankfurt Institute for Advanced Studies, Frankfurt, Germany*
[2]*Institute for Theoretical and Experimental Physics, Moscow, Russia*
(Received 20 June 2008; published 5 September 2008)

The low p_T direct photon production from a variety of the hadronic sources is studied within the microscopic hadron-string dynamics transport approach for $p + \mathrm{C}$, $p + \mathrm{Pb}$, and $\mathrm{Pb} + \mathrm{Pb}$ collisions at 160A GeV. The direct photon emission from elementary hadronic scatterings as well as meson-meson bremsstrahlung are incorporated. The influence of in-medium effects such as a collisional broadening of the vector-meson spectral functions on the photon emission rate is found to be hardly observable in the final spectra that are dominated by bremsstrahlung-type processes. The uncertainties in the subtraction of the "background" from the photon decay of hadronic resonances inside the hot and dense fireball is investigated, additionally. Our findings are relevant for the interpretation and extraction of experimental data on direct photon production at low p_T.

DOI: 10.1103/PhysRevC.78.034905 PACS number(s): 25.75.Cj, 24.10.Lx

I. INTRODUCTION

The properties of hadronic matter under extreme densities and temperatures and their phase transition to the deconfined and strongly interacting quark-gluon plasma (QGP) are the central topics of modern high-energy physics. To understand the dynamics and relevant scales of this transition laboratory experiments under controlled conditions are presently performed with ultrarelativistic nucleus-nucleus collisions. The electromagnetic radiation (real and virtual photons, i.e., dilepton pairs) is the unique probe to study the heavy-ion collisions because the photons do not suffer from the final-state interactions with the surrounding matter and, thus, provide a clear signal of the various environments of their creations (cf. the pioneering works [1–3]). Moreover, the photons are emitted from all stages of the collisions, from the QGP to the hadronic phase, so they may provide information about the different degrees of freedom from partons to hadrons [4–7].

On the quark-gluon level the main processes for the direct photon production are Compton scattering of quarks and gluons $qg \to q\gamma$ and annihilation of quark and antiquarks $q\bar{q} \to g\gamma$ as leading processes, whereas the next-to-leading-order (NLO) process is dominated by bremsstrahlung $qg \to qg\gamma$. The photons radiated from the different sources have a different transverse momentum p_T that allows us to separate the contributions: The photons with high p_T are primarily produced by the initial hard NN collisions and called as "prompt" (or "hard") photons. Direct photons from a thermalized QGP dominate at lower transwerse momentum ($1 \leqslant p_T \leqslant 3$ GeV/c) and denoted as "thermal photons." On the hadronic level the main source of direct photons is meson-meson rescattering: $\pi\rho \to \pi\gamma, \pi\pi \to \rho\gamma, \pi K \to K^*\gamma, K\rho \to K\gamma, \ldots$, where the first two channels are the most important. These photons from the hadronic rescattering dominate at even lower p_T. Additionally there are photons coming from the hadron decays (such as π^0, η, etc.), which give a huge photonic "background" and make the experimental measurement of direct photons very complicated.

Most of the theoretical predictions for direct photons are based on the local thermalization assumption and evaluate the photon production rates from the equilibrated quark-gluon plasma or hadronic matter that then are convoluted with the space-time evolution of the system. To account for the nonequilibrium dynamics with its full complexity one needs microscopic transport models. However, most of the transport models commonly used for the description of high energy heavy-ion collisions are based on the hadron-string picture (e.g., hadron string dynamics (HSD) transport approach and ultrarelativistic quantum molecular dynamics (UrQMD)) and do not include the phase transition from partonic to hadronic matter in a consistent way, nor do they solve the hadronization problem. We mention that there are attempts to develop such transport models, e.g., the multiphase transport model (AMPT) [8], which includes perturbative quantum chromodynamics-like (pQCD) partonic scattering, combined models, such as hydrodynamics for the QGP+UrQMD for the hadronic stage [9], or the parton-hadron-string-dynamics (PHSD) model that is based on a dynamical quasiparticle model matched to reproduce lattice QCD results in thermodynamic equilibrium [10].

We recall that as early as 1995–1997 there were attempts to describe the first experimental photon data by WA98 Collaboration on $\mathrm{S} + \mathrm{Au}$ at 200A GeV [11] in the transport models UrQMD [12], AMPT [13], and HSD [14]. The transport calculations included the photon production by the hadronic decays [12–14] as well as direct photon production from the meson-meson scattering [12,13]. Also the influence of in-medium effects such as dropping vector-meson masses on the photon yield have been addressed in Refs. [13,14]. Unfortunately, the first WA98 data provided only an upper bound for the direct photon production yield and did not allow to draw solid conclusions; all transport results were just below the upper limit given by WA98. In 2000 the WA98 Collaboration provided new data for $\mathrm{Pb} + \mathrm{Pb}$ at 160A GeV [15]. This stimulated a new wave of interest for direct photons from the theoretical side (cf. Ref. [16] and references therein).

The aim of our present study is to investigate the photon production at CERN Super Proton Synchrotron (SPS) energies from hadronic sources using the extended version of the HSD transport model [17,18] that includes the off-shell dynamics of the vector mesons with dynamical spectral functions. It allows

us to study the influence of in-medium effects—such as a collisional broadening—on the photon emission rate. We will compare our transport calculations to the experimental data for Pb + Pb at 160A GeV as well as to the new preliminary data on photon production in p + C and p + Pb collisions at 160A GeV [19]. We stress here again that the HSD model does not include the phase transition from QGP to hadronic matter; we thus concentrate on the low p_T photon production that is dominated by hadronic sources. First "pilot" HSD results have been reported in Ref. [20].

Our paper is organized as follows: In Sec. II we describe the treatment of various channels for the photon production in HSD. Section III contains a comparison of the HSD results with the WA98 data for Pb + Pb at 160A GeV, whereas Sec. IV contains our results for photon production in p + C and p + Pb collisions at 160A GeV. A summary closes this work in Sec. V.

II. PHOTON PRODUCTION IN HSD

Our analysis is carried out within the HSD transport model [14,21,22], based on covariant self-energies for the baryons [23], that has been used for the description of pA and AA collisions from GSI Schwerionen Synchrotron (SIS) to Relativistic Heavy Ion Collider (RHIC) energies. We recall that in the HSD approach nucleons, Δ's, N*(1440), N*(1535), Λ, Σ, and Σ^* hyperons, Ξ's, Ξ^*'s, and Ω's as well as their antiparticles are included on the baryonic side, whereas the 0^- and 1^- octet states are incorporated in the mesonic sector. Inelastic baryon-baryon (and meson-baryon) collisions with energies above $\sqrt{s}_{\rm th} \simeq 2.6$ GeV (and $\sqrt{s_{\rm th}} \simeq 2.3$ GeV) are described by the FRITIOF string model [24], whereas low-energy hadron-hadron collisions are modeled in line with experimental cross sections. Note that the HSD transport approach includes the off-shell dynamics of vector mesons explicitly; for the details we address the reader to Ref. [17].

We consider the following hadronic sources of photon production:

(i) The photon production by a mesonic decays (π^0, η, η', ω, ϕ, a_1) where the mesons are produced first in baryon-baryon (BB), meson-baryon (mB), or meson-meson (mm) collisions. The photon production from the mesonic decays represents a "background" for the search of the direct photons; however, this background is very large relative to the expected direct photon signal. Moreover, there are severe experimental difficulties in subtracting the photons from hadronic decays. For the present study we consider the contributions from the photon decay of the following mesons:

$$\begin{aligned} \pi^0 &\to \gamma + \gamma, \\ \eta &\to \gamma + \gamma, \\ \eta' &\to \rho + \gamma, \\ \omega &\to \pi^0 + \gamma, \\ \phi &\to \eta + \gamma, \\ a_1 &\to \pi + \gamma. \end{aligned} \tag{1}$$

The decay probability is calculated according to the corresponding branching ratios taken from PDG [25]. The broad resonances in the initial/final state are treated in line with their in-medium spectral functions that will be illustrated in the next subsections.

(ii) Additionally to the resonance/meson decay channels the photons can be produced directly in elementary collisions of particles. For the present study we consider the direct photon production by the scattering processes

$$\pi\pi \to \rho\gamma, \tag{2}$$

$$\pi\rho \to \pi\gamma, \tag{3}$$

accounting for all possible charge combinations. We note that we discard γ production in rescattering processes with strange mesons (such as $\pi + K^* \to K + \gamma$, $\pi + K \to K^* + \gamma$, $K + K^* \to \pi + \gamma$ etc.), because at SPS energies the strange meson density is subdominant. However, as indicated in Ref. [26], such processes may play a role at higher energies. In the next subsections we will define the contributions of the processes $\pi\pi \to \rho\gamma$, $\pi\rho \to \pi\gamma$ explicitly.

(iii) The photon production from meson-meson bremsstrahlung might play an important role, too, as has been pointed out first by Haglin [27] and later by Liu and Rapp [28]. These authors have calculated the thermal photon emission rate from the proceses $m + m \to m + m + \gamma$ and found that the bremsstrahlung radiation is one of the dominant channels for low-energy photon production.

In the next subsections we define explicitly the treatment of the dominant hadronic process for direct photon production.

A. Direct photon production in $\pi\pi \to \rho\gamma$ reactions

Because at SPS energies the pion density is relatively high, the $\pi\pi$ annihilation channel has to be accounted for in the direct photon production. With increasing energies (and pion densities) the importance of this channel grows accordingly.

The basic form of the cross section for the $\pi\pi \to \rho\gamma$ reaction has been adopted from Kapusta *et al.* in Ref. [29], where the high-energy photon production has been evaluated in the hot hadron gas model. However, in Ref. [29] the final ρ meson has been considered on-shell, i.e., at the pole mass $M_0 = 0.77$ GeV. Because in HSD the vector mesons are treated with the full off-shell spectral function, which depends on density and momentum [17], some modification of the formulas from Ref. [29] has to be done to account for the broad mass distribution of the final ρ meson. The simplest way is to "fold" the cross section from Ref. [29] with the mass- and density-dependent spectral function of the ρ mesons.

We note that for the present study we use the same form of spectral functions for the vector mesons as modeled in Ref. [17]. In particular, the spectral function of a vector meson V with mass M at nucleon density ρ_N is taken in the

Breit-Wigner form:

$$A_V(M,\rho_N) = C_1 \cdot \frac{2}{\pi} \frac{M^2 \Gamma_V^*(M,\rho_N)}{[M^2 - M_0^{*2}(\rho_N)]^2 + [M\Gamma_V^*(M,\rho_N)]^2}, \quad (4)$$

with the normalization condition for any ρ_N:

$$\int_{M_{\rm min}}^{M_{\rm lim}} A_V(M,\rho_N)\, dM = 1, \quad (5)$$

where $M_{\rm lim} = 2$GeV is chosen as an upper limit for the numerical integration. The lower limit of the vacuum ρ spectral function corresponds to the 2π decay $M_{\rm min} = 2m_\pi$, whereas for the in-medium collisional broadening case $M_{\rm min} = 2m_e \to 0$ with m_e denoting the electron mass. M_0^* is the pole mass of the vector-meson spectral function that is $M_0^*(\rho_N = 0) = M_0$ in vacuum, however, shifted in the medium for the dropping mass scenario according to the Hatsuda and Lee [30] or Brown/Rho scaling [31]. Futhermore, the vector-meson width has been implemented as:

$$\Gamma_V^*(M, |\vec{p}|, \rho_N) = \Gamma_V(M) + \Gamma_{\rm coll}(M, |\vec{p}|, \rho_N). \quad (6)$$

Here $\Gamma_V(M)$ is the total width of the vector mesons ($V = \rho, \omega$) in the vacuum. For the ρ meson we use

$$\Gamma_\rho(M) \simeq \Gamma_{\rho\to\pi\pi}(M) = \Gamma_0 \left(\frac{M_0}{M}\right)^2 \left(\frac{q}{q_0}\right)^3 F(M)$$
$$q = \frac{\left(M^2 - 4m_\pi^2\right)^{1/2}}{2}, \quad q_0 = \frac{\left(M_0^2 - 4m_\pi^2\right)^{1/2}}{2}. \quad (7)$$

In Eq. (7) Γ_0 is the vacuum width of the ρ meson at the pole mass M_0; $F(M)$ is a form factor taken from Ref. [32] as

$$F(M) = \left(\frac{2\Lambda^2 + M_0^2}{2\Lambda^2 + M^2}\right)^2 \quad (8)$$

with a cut-off parameter $\Lambda = 3.1$ GeV. This form factor was introduced in Ref. [32] to describe the e^+e^- experimental data. For the ω meson a constant total vacuum width is used: $\Gamma_\omega \equiv \Gamma_\omega(M_0)$, because the ω is a narrow resonance in vacuum.

The collisional width in Eq. (6) is approximated as

$$\Gamma_{\rm coll}(M, |\vec{p}|, \rho_N) = \gamma \rho_N \langle v\, \sigma_{VN}^{\rm tot} \rangle \approx \alpha_{\rm coll} \frac{\rho_N}{\rho_0}. \quad (9)$$

Here $v = |\vec{p}|/E$; $\vec{p}$, E are the velocity, three-momentum, and energy of the vector meson in the rest frame of the nucleon current and $\gamma^2 = 1/(1 - v^2)$. Furthermore, $\sigma_{VN}^{\rm tot}$ is the meson-nucleon total cross section.

As discussed in Ref. [17], to simplify the actual calculations, the coefficient $\alpha_{\rm coll}$ has been extracted in the HSD transport calculations from the vector-meson collision rate in $A + A$ reactions as a function of the density ρ_N. The numerical results for $\Gamma_{\rm coll}(\rho_N)$ then have been divided by ρ_N/ρ_0 to fix the coefficient $\alpha_{\rm coll}$ in Eq. (9). We obtain $\alpha_{\rm coll} \approx 150$ MeV for the ρ and $\alpha_{\rm coll} \approx 70$ MeV for ω mesons that are consistent with the experimental analysis in Ref. [33]. In this way the average effects of collisional broadening are incorporated and allow for an explicit representation of the vector-meson spectral functions versus the nuclear density, ρ_N.

We mention that also finite temperature effects lead to a sizable broadening of the vector-meson spectral functions (also at baryon chemical potential $\mu_B = 0$). This is essentially due to scattering with mesons that may contribute to the total width by 70–80 MeV at a temperature of $\sim$170 MeV according to the early work by Haglin [34]. But for the present study we use a simplified modeling of the collisional broadening width that discards an explicit consideration of such temperature effects. However, the temperature effects are partly accounted here due to explicit meson-meson interactions that also lead to changes in the vector-meson mass distribution. Because we find that the spectral broadening of the mesons is practically not visible in the final photon spectra, an explicit consideration of temperature effects is beyond the scope of this study.

To explore the observable consequences of vector-meson mass shifts at finite nuclear density—as indicated by the CBELSA-TAPS data [35] for the ω meson—the in-medium vector-meson pole masses are modeled (optionally) according to the Hatsuda and Lee [30] or Brown/Rho scaling [31] as

$$M_0^*(\rho_N) = \frac{M_0}{(1 + \alpha\rho_N/\rho_0)}, \quad (10)$$

where ρ_N is the nuclear density at the resonance decay position $\vec{r}$, $\rho_0 = 0.16$ fm^{-3} is the normal nuclear density, and $\alpha \simeq 0.16$ for the ρ and $\alpha \simeq 0.12$ for the ω meson [33]. The parametrization (10) may be employed also at much higher collision energies (e.g., Facility for Antiproton and Ion Research and SPS) and one does not have to introduce a cut-off density to avoid negative pole masses. Note that Eq. (10) is uniquely fixed by the "customary" expression $M_0^*(\rho_N) \approx M_0(1 - \alpha\rho_N/\rho_0)$ in the low-density regime.

Thus, we model the photon ρ-meson production cross section in $\pi\pi$ reactions in the following way: the total cross section $\sigma_{\pi\pi\to\rho\gamma}(s, \rho_N)$ is

$$\sigma_{\pi\pi\to\rho\gamma}(s,\rho_N) = \int_{M_{\rm min}}^{M_{\rm max}} dM\, \frac{d\sigma_{\pi\pi\to\rho\gamma}(s, M, \rho_N)}{dM}. \quad (11)$$

The mass differential cross section is approximated by

$$\frac{d\sigma_{\pi\pi\to\rho\gamma}(s, M, \rho_N)}{dM} = \sigma^0_{\pi\pi\to\rho\gamma}(s, M) \times A(M, \rho_N) \times \frac{\int_{M_{\rm min}}^{M_{\rm max}} A(M,\rho_N) dM}{\int_{M_{\rm min}}^{M_{\rm lim}} A(M,\rho_N) dM}, \quad (12)$$

where $A(M, \rho_N)$ denotes the meson spectral function (4) for given total width Γ_V^* (6); $M_{\rm max} = \sqrt{s}$ is the maximal kinematically allowed invariant mass of the ρ meson. In Eq. (12) $\sigma^0_{\pi\pi\to\rho\gamma}(s, M)$ is the vacuum cross section from Kapusta *et al.* [29] where the ρ-meson mass is considered as a free variable (i.e., not fixed to 0.77 GeV as in Ref. [29]). Thus, formula (12) can be used to model the vector-meson production in $\pi\pi$ reactions in the vacuum and in the medium, too.

Figure 1 shows the γ-production cross section $\sigma(s, \rho)$ for the $\pi^- + \pi^0 \to \rho^- + \gamma$, $\pi^+ + \pi^0 \to \rho^+ + \gamma$ (upper part), and $\pi^+ + \pi^- \to \rho^0 + \gamma$ (lower part) reaction for $\rho_N = 0$ (solid lines) and in case of the "collisional broadening" scenario (dashed lines) and the "dropping mass + collisional broadening" scenario (short dashed lines) for nuclear density

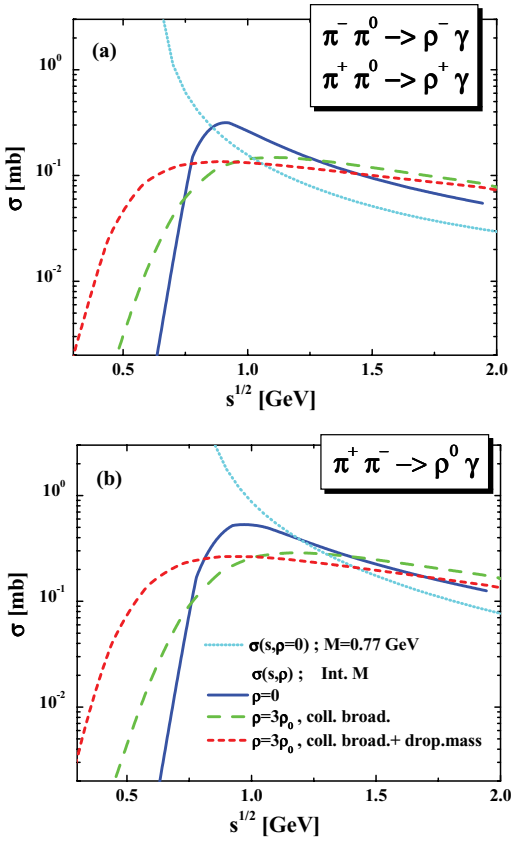

FIG. 1. (Color online) The γ-production cross section $\sigma(s, \rho)$ for the $\pi^- + \pi^0 \to \rho^- + \gamma, \pi^+ + \pi^0 \to \rho^+ + \gamma$ (a) and $\pi^+ + \pi^- \to \rho^0 + \gamma$ (b) reaction for $\rho_N = 0$ (solid lines) and in the case of the "collisional broadening" scenario (dashed lines) and the "dropping mass + collisional broadening" scenario (short dashed lines) for nuclear density $\rho_N = 3\rho_0$. The dotted lines correspond to the results from Kapusta *et al.* [29] for the fixed ρ-meson mass $M = 0.77$ GeV, whereas all other lines show the yield integrated over the ρ-meson mass M.

$\rho_N = 3\rho_0$. The dotted lines correspond to the original cross section from Kapusta *et al.* [29] for the fixed ρ-meson mass $M = 0.77$ GeV, whereas all other lines show the cross section integrated over the mass M. Note that the cross section from Kapusta *et al.* [29] for the fixed ρ-meson mass diverges at threshold. However, the folding over the spectral function of the ρ meson leads to an endothermic behavior of the cross section (cf. the solid line) instead of an exothermic (dotted line).

As seen from Fig. 1 the cross section in the 'collisional broadening' scenario is basically smeared out close to threshold. Only when incorporating additionally a dropping mass the thresholds are shifted down in energy such that the production cross sections become enhanced in the subthreshold regime with increasing nuclear density ρ_N.

B. Direct photon production in $\pi\rho \to \pi\gamma$ reactions

In Fig. 2 we show the production cross section $\sigma(s)$ for the $\pi^- + \rho^0 \to \pi^- + \gamma, \pi^+ + \rho^0 \to \pi^+ + \gamma$ (upper part),

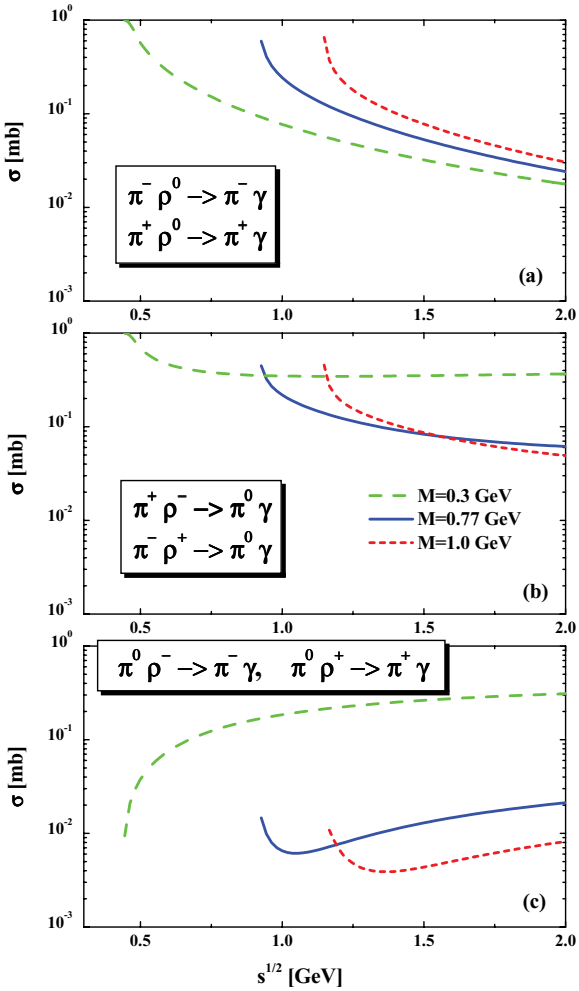

FIG. 2. (Color online) The production cross section $\sigma(s)$ for the $\pi^- + \rho^0 \to \pi^- + \gamma, \pi^+ + \rho^0 \to \pi^+ + \gamma$ (a), $\pi^+ + \rho^- \to \pi^0 + \gamma, \pi^- + \rho^+ \to \pi^0 + \gamma$ (b), and $\pi^0 + \rho^- \to \pi^- + \gamma, \pi^0 + \rho^+ \to \pi^+ + \gamma$ (c) reaction. The dashed lines corresponds to the ρ-meson mass $M = 0.3$ GeV, the solid lines stand for $M = 0.77$ GeV, and the short dashed lines correspond to $M = 1.0$ GeV.

$\pi^+ + \rho^- \to \pi^0 + \gamma, \pi^- + \rho^+ \to \pi^0 + \gamma$ (middle part), and $\pi^0 + \rho^- \to \pi^- + \gamma, \pi^0 + \rho^+ \to \pi^+ + \gamma$ (lower part) reactions. Here again we use the vacuum cross sections from Kapusta *et al.* [29] and consider the ρ-meson mass as a free variable because the production of the vector mesons in HSD is realized with respect to the spectral function $A(M, \rho_N)$. The dashed lines corresponds to the ρ-meson mass $M = 0.3$ GeV, the solid lines stand for $M = 0.77$ GeV, whereas the short dashed lines correspond to $M = 1.0$ GeV.

As follows from Fig. 2 the $\pi + \rho \to \pi + \gamma$ cross section depends very strongly on the mass of the initial ρ meson—for low M the threshold is shifted to low $\sqrt{s}$. Thus, one can expect an enhancement of γ production in case of this channel for the in-medium scenarios due to the enhanced population of the low-mass ρ mesons.

C. Photon production by the decay $a_1 \to \pi\gamma$

The photons can be also emitted from the decay $a_1 \to \pi\gamma$. Despite the fact that the branching ratio of this process is not well known experimentally and expected to be very small (we use $\mathrm{Br}(a_1 \to \pi\gamma) \sim 1.5 \times 10^{-3}$ [36]), this contribution is also considered in our investigation. The study of the a_1 dynamics is an interesting problem itself because it is related to chiral symmetry restoration at high densities and temperatures as pointed out in Refs. [37–40].

The production of a_1 mesons in HSD stems from BB and mB collisions via string excitation and decay at high energies and by $\pi + \rho \leftrightarrow a_1$ reactions at low energies. The mass of the a_1 meson is distributed according to the Breit-Wigner spectral function [Eq. (4)] with a mass- (μ) and density- (ρ_N) dependent width $\Gamma^*_{a_1}$. The total a_1 width Γ_{a_1} can be written as

$$\Gamma^*_{a_1}(\mu, |\vec{p}|, \rho_N) = \Gamma_{a_1}(\mu, \rho_N) + \Gamma_{a_1:\mathrm{coll}}(\mu, |\vec{p}|, \rho_N), \quad (13)$$

where the collisional width is approximated by $\Gamma_{a_1:\mathrm{coll}}(\mu, |\vec{p}|, \rho_N) \simeq \alpha_{a_1:\mathrm{coll}} \rho_N/\rho_0$ with $\alpha_{a_1:\mathrm{coll}} \simeq 150$ MeV.

Because the a_1 meson decays dominantly to $\pi + \rho$ [39] one has to take into account the mass distribution of the final ρ meson $A(M, \rho_N)$ when calculating the width of the a_1 meson. Thus formula (7) for the a_1 width $\Gamma_{a_1}(\mu, \rho_N)$ has to be modified accordingly:

$$\begin{aligned}
\Gamma_{a_1}(\mu, \rho_N) &= \Gamma^0_{a_1} \left(\frac{\mu_0}{\mu}\right)^2 \\
&\quad \times \frac{\int_{M_{\min}}^{\mu - m_\pi} dM\, q^3(\mu, M)\, A(M, \rho_N)}{\int_{M_{\min}}^{\mu_0 - m_\pi} dM\, q_0^3(\mu_0, M)\, A(M, \rho_N)}; \\
q(\mu, M) &= \frac{\sqrt{\lambda(\mu, M, m_\pi)}}{2\mu}, \\
q_0(\mu_0, M) &= \frac{\sqrt{\lambda(\mu_0, M, m_\pi)}}{2\mu_0}.
\end{aligned} \quad (14)$$

Here $\lambda(x, y, z) = [x^2 - (y - z)^2][x^2 - (y + z)^2]$, whereas m_π is the pion mass; $\mu_0, \Gamma^0_{a_1}$ are the vacuum pole mass and width of the a_1 spectral function with $\Gamma^0_{a_1}$ taken as 400 MeV.

According to Eq. (14) the a_1 width depends on the ρ meson spectral function $A(M, \rho_N)$ and, thus, is sensitive to the ρ meson in-medium effects. We stress, that such a "coupling" of the a_1 and ρ spectral functions has to be accounted for when drawing conclusions about an experimental observation of chiral symmetry restoration by measuring the a_1 meson properties in heavy-ion experiments (e.g., the corresponding results in Ref. [40] should be strongly affected).

Figure 3 shows the spectral function $A_{a_1}(\mu, \rho_N)$ for the a_1 meson for $\rho_N = 0$ (solid line) and in the case of the collisional broadening scenario (dashed line) and the dropping mass + collisional broadening scenario (short dashed line) for nuclear density $\rho_N = 3\rho_0$. Here the in-medium scenarios are related to both the a_1 as well as the ρ meson.

The production cross section $\sigma(s, M)$ for the $\pi + \rho \to a_1$ reaction (for all possible charge combinations) is calculated as follows,

$$\sigma_{\pi+\rho\to a_1}(s, M, \rho_N) = \frac{6\pi^2}{q^2(s, M)} \Gamma_{a_1}(s, \rho_N) A_{a_1}(s, \rho_N), \quad (15)$$

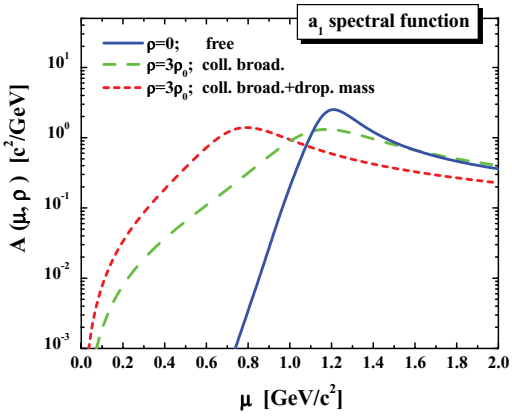

FIG. 3. (Color online) The spectral function for the a_1 meson for $\rho_N = 0$ (solid line) and in case of the "collisional broadening" scenario (dashed line) and the "dropping mass + collisional broadening" scenario (short dashed line) for nuclear density $\rho_N = 3\rho_0$.

where $s \equiv \mu^2$ and the width $\Gamma_{a_1}(s, \rho_N)$ and momentum $q(s, M)$ are defined by Eq. (14).

In Fig. 4 we display the production cross section $\sigma(s, M)$ for the $\pi + \rho \to a_1$ reaction for $\rho_N = 0$ (solid lines) and in case of the collisional broadening scenario (dashed lines) and the dropping mass + collisional broadening scenario (short dashed lines) for nuclear density $\rho_N = 3\rho_0$. The upper part corresponds to the ρ-meson mass of $M = 0.77$ GeV, whereas the lower part shows the results for $M = 0.3$ GeV. As seen from Fig. 4 the a_1 production cross section in the $\pi + \rho$ reaction is very sensitive to the in-medium scenarios as well as to the mass M of the initial ρ meson (even in the free case —cf. solid lines).

D. Direct photon production from meson-meson bremsstrahlung

The implementation of photon bremsstrahlung from hadronic reactions in transport approaches is based on the "soft photon" approximation. The soft-photon approximation (SPA) [41] relies on the assumption that the radiation from internal lines is negligible and the strong interaction vertex is on-shell. In this case the strong interaction part and the electromagnetic part can be separated, so the soft-photon cross section for the reaction $1 + 2 \to 1 + 2 + \gamma$ can be written as

$$\begin{aligned}
q_0 \frac{d^3\sigma^\gamma}{d^3q} &= \frac{\alpha}{4\pi} \frac{\bar{\sigma}(s)}{q_0^2} \\
\bar{\sigma}(s) &= \frac{s - (M_1 + M_2)^2}{2M_1^2} \sigma(s),
\end{aligned} \quad (16)$$

where M_1 is the mass of the charged accelerated particle, M_2 is the mass of the second particle, and q_0, q are the energy and momentum of the photon. In Eq. (16) $\sigma(s)$ is the on-shell elastic cross section for the reaction $1 + 2 \to 1 + 2$. This approximation has also been employed by Haglin in Ref. [27].

In Ref. [28] the photon bremsstrahlung from $\pi + \pi$ and $\pi + K$ elastic collisions has been calculated using the $U_{\mathrm{em}}(1)$-gauged meson-exchange model that includes the photon

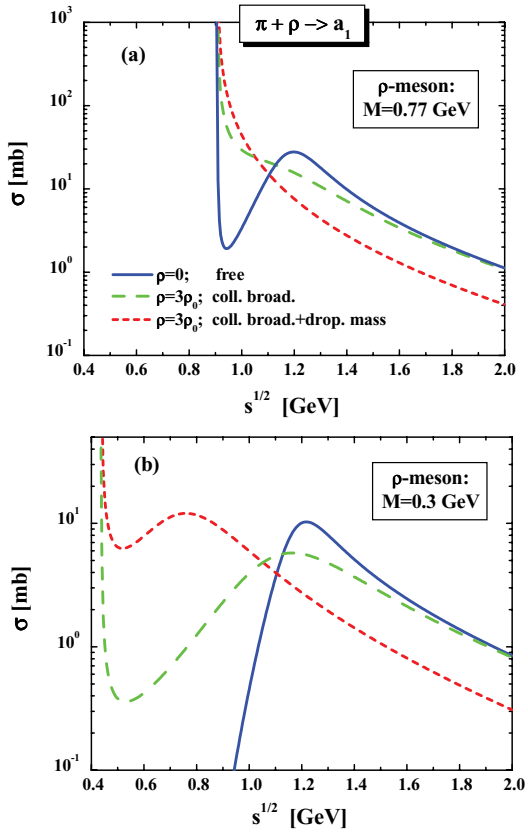

FIG. 4. (Color online) The production cross section $\sigma(s, M)$ for the $\pi + \rho \to a_1$ reaction for $\rho_N = 0$ (solid lines) and in the case of the collisional broadening scenario (dashed lines) and the dropping mass + collisional broadening scenario (short dashed lines) for nuclear density $\rho_N = 3\rho_0$. The upper part (a) corresponds to $M =$ 0.77 GeV, whereas the lower part (b) shows the results for $M =$ 0.3 GeV.

coupling to pseudoscalar and vector mesons. Indeed, such calculations go beyond the SPA model. However, the direct comparison of SPA and the $U_{\rm em}(1)$ models—cf. Fig. 4 in Ref. [28]—show a very good agreement between the models, which allows us to use the simplified SPA formula for our purpose here. Thus, we have calculated the photon bremsstrahlung from all elastic meson-meson scattering $m_1 + m_2 \to m_1 + m_2 + \gamma$ (where $m = \pi, \eta, K, \bar{K}, K^0, K^*, \bar{K}^*, K^{*0}$), which occur during the heavy-ion collisions by applying the SPA formula (16).

III. RESULTS FOR THE PHOTON PRODUCTION IN $A + A$ COLLISIONS AT SPS ENERGIES

Now we step on to the description of direct photon production from heavy-ion collisions applying the HSD transport model incorporating all photon production channels from elementary reactions as described in the previous section.

In Fig. 5 we start with a comparison of the HSD results for the inclusive photon transverse momentum distribution for 10% central 158A GeV ^{208}Pb + ^{208}Pb collisions with the experimental data from the WA98 Collaboration [15] (solid dots). We select photons in the pseudorapidity interval

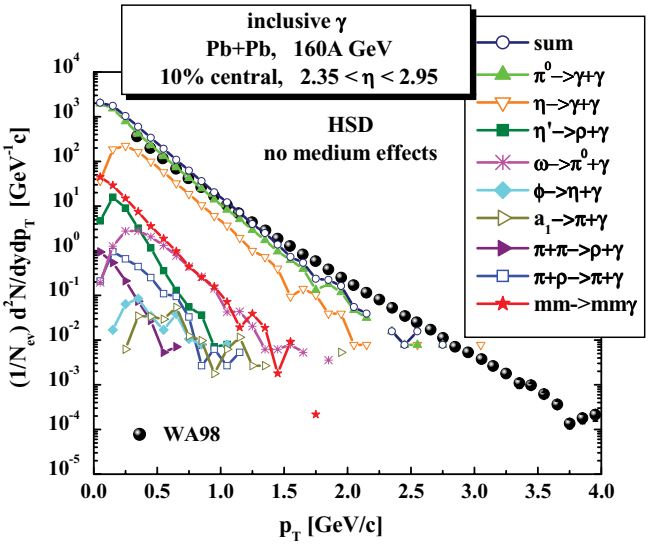

FIG. 5. (Color online) The inclusive photon transverse-momentum distribution for central 158A GeV ^{208}Pb + ^{208}Pb collisions at $2.35 \leqslant \eta \leqslant 2.95$. The solid symbols and arrows corresponds to the WA98 data [15], and the lines correspond to the HSD results for the various channels as indicated in the legend (without medium effects for the vector mesons).

$2.35 \leqslant \eta \leqslant 2.95$ in the laboratory frame that corresponds to midrapidity in the center-of-mass frame. Our calculations show that such a cut in pseudorapidity reduces the photon yield by about of factor 5; however, it does not really change the shape of the p_T spectra. The WA98 data correspond to the transverse-momentum interval $0.5 \leqslant p_T \leqslant 4$ GeV/c, whereas the HSD calculation includes also very low p_T momenta but extends up to 2.5-3 GeV/c only because the high p_T tail is very hardly reachable due to limitied statistics.

Figure 5 presents the HSD calculations without medium effects for the vector mesons (the definition of the lines are indicated in the legend). As seen from Fig. 5 the dominant channels for the inclusive photon production are the photon from π and η decays ($\pi \to \gamma + \gamma$ and $\eta \to \gamma + \gamma$), whereas other channels are down by more than order of magnitude. The HSD results agree very well with the experimental data that is, indeed, expectable because the HSD model provides a good description of the pion transverse-momentum spectra at SPS energies [42] and predicts a meson m_T scaling [43].

To obtain the information about the direct photon production, one needs to subtract the "background" contributions that are dominated by the mesonic decay processes. Although the π^0 and η spectra are measured directly by the same experiments [15], it is possible to estimate their photon decay in a reliable way. Indeed, the lifetimes of π's and η's are large such that they basically decay at the end of reaction stage, i.e., in vacuum. However, the situation with the $\eta' \to \rho + \gamma, \omega \to \pi^0 + \gamma, \phi \to \eta + \gamma, a_1 \to \pi + \gamma$ decays are not so transparent because these mesons cannot be mesured directly by the WA98 detector.

The WA98 Collaboration has subtracted the contribution of hadronic decays by calculations based on the assumption of m_T scaling with the same slope of the m_T spectra as

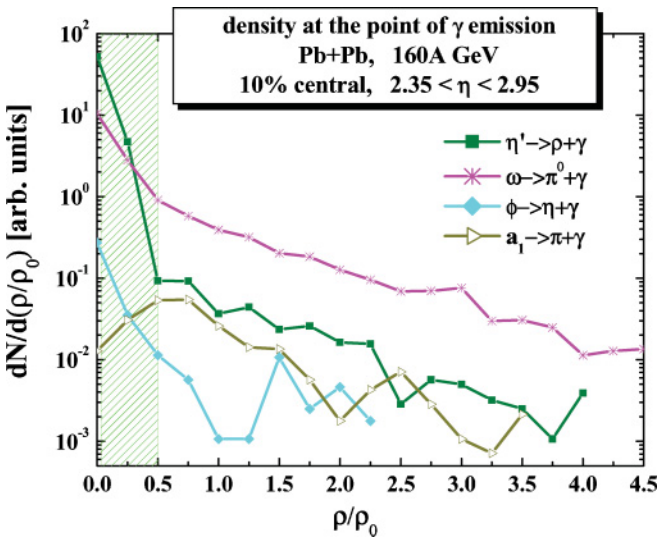

FIG. 6. (Color online) The nucleon density distribution at the photon emission point (in units of ρ_0) for central 158A GeV ^{208}Pb + ^{208}Pb collisions at $2.35 \leqslant \eta \leqslant 2.95$. The definition of the lines is indicated in the legend.

measured in the π^0 spectrum and with relative normalizations R_{hadron/π^0} (equivalent to the asymptotic ratios for $p_T \to \infty$) [15]. However, such a procedure is a rough approximation especially for the short living resonances that can emit photons inside the hot fireball shortly after creation and, thus, cannot be reconstruct in experiment. This statement is illustrated in Fig. 6 that shows the density distribution at the photon emission points from η', ω, ϕ, a_1 decays for central 158A GeV ^{208}Pb + ^{208}Pb collisions at $2.35 \leqslant \eta \leqslant 2.95$. One can see from Fig. 6 that there is some fraction of ω, ϕ, a_1 mesons that emit photons for $\rho_N \geqslant \rho_0/2$ (e.g., ∼25% of ω's and ∼70% of a_1's), whereas a relatively long leaving η' meson decays dominantly at low densities.

To demonstrate the possible contribution of the in-medium decays of η', ω, ϕ, a_1 mesons to the direct photon spectra reported by the WA98 Collaboration we show in the right-hand side of Fig. 7 the invariant midrapidity spectra including the contribution of the η', ω, ϕ, a_1 photon decay only for $\rho_N > \rho_0/2$, whereas the left-hand side of Fig. 7 shows the total contribution of all hadronic channels at all densities (for comparison). Indeed, such a cut in density leads to a substantial reduction of the hadronic decay 'background' especially for low p_T, however, it becomes essential at $p_T \leqslant 0.7$ GeV/c. Thus, our calculations provide the scale of possible uncertainties in the experimental background subtraction which is important for the physical interpretation of the experimental results.

One can see from Fig. 7 that the dominant channel for low p_T photon production is meson-meson bremsstrahlung. This is in line with the analysis by Haglin [27] and Liu

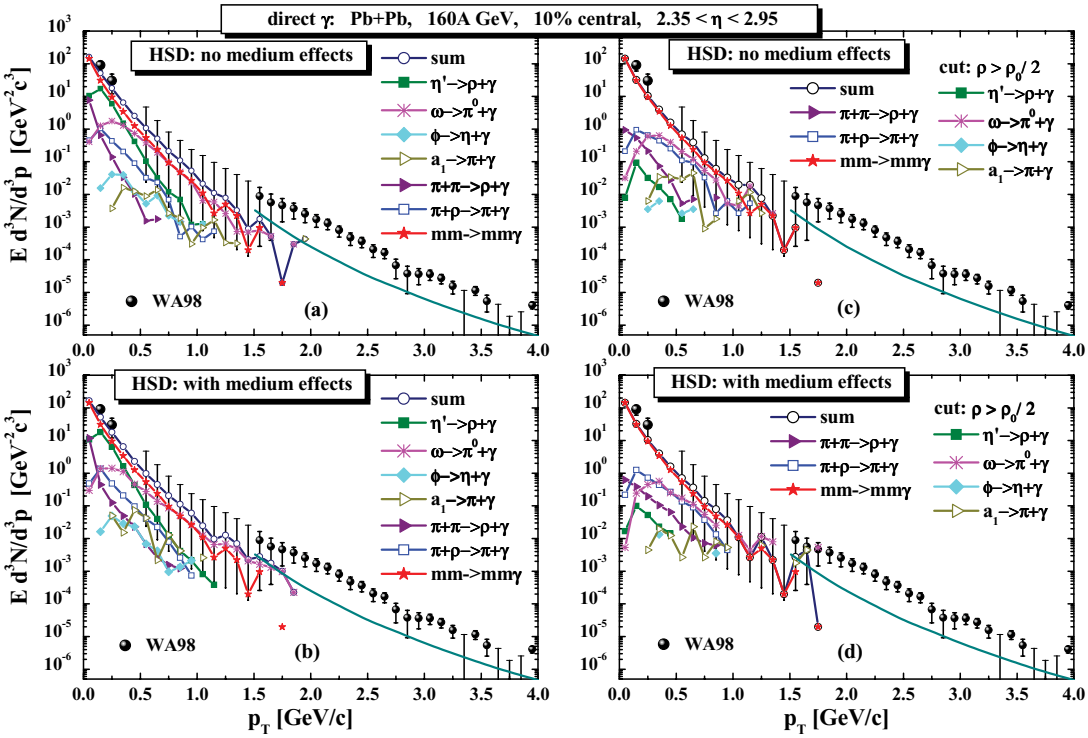

FIG. 7. (Color online) The invariant direct photon multiplicity for central 158A GeV ^{208}Pb + ^{208}Pb collisions at $2.35 \leqslant \eta \leqslant 2.95$. The solid symbols and arrows corresponds to the WA98 data [15], the lines stand for the HSD calculations without [upper row, (a) and (c)] and with [lower row, (b) and (d)] medium effects (i.e., collisional broadening) for the vector mesons. The definition of the lines is indicated in the legend. The solid line for $p_T > 1.5$ GeV/c gives the contribution from the prompt photons. The right panel [(c) and (d)] shows the spectra including the contribution of the η', ω, ϕ, a_1 photon decay only for $\rho_N > \rho_0/2$, whereas the left panel [(a) and (b)] shows the total contribution of all hadronic channels at all densities.

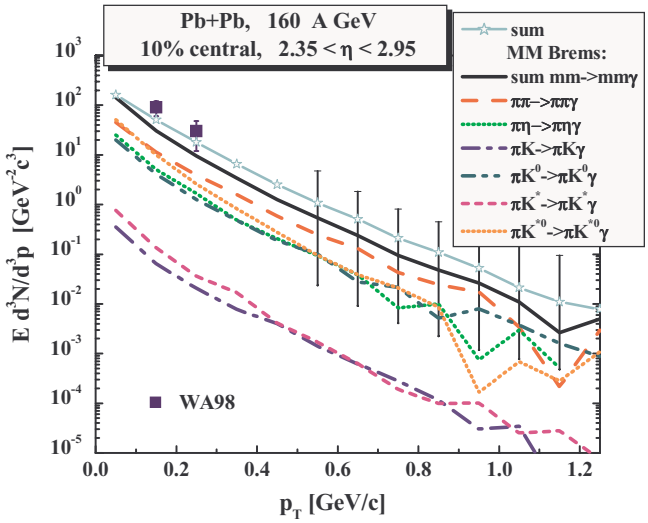

FIG. 8. (Color online) The invariant direct photon multiplicity for central 158A GeV ^{208}Pb + ^{208}Pb collisions at $2.35 \leqslant \eta \leqslant 2.95$. The solid symbols and arrows corresponds to the WA98 data [15], the lines stand for the HSD calculations: the upper solid line with the stars shows the sum over all channels, the solid line corresponds to the sum over all meson-meson bremsstrahlung channels that are specified by the various lines. The definition of the lines is indicated in the legend.

and Rapp [28]. The contributions of the other channels, such as direct photon production by meson-meson collisions $\pi + \pi \to \rho + \gamma$ and $\pi + \rho \to \pi + \gamma$, are found to be suppressed relative to the meson-meson bremsstrahlung. Also we have investigated the influence of in-medium effects such as collisional broadening for the vector-meson spectral functions that lead (e.g.) to enhancement of low-mass dilepton production [17,18]. However, we here obtain only a small affect on the direct photon production that is hidden below the dominant bremsstrahlung contribution. The same holds also for other in-medium scenario such as a dropping mass of the vector meson.

In Fig. 8 we specify the meson-meson bremsstrahlung by showing the contributions of different subchannels $\pi + \pi \to \pi + \pi + \gamma, \pi + \eta \to \pi + \eta + \gamma, \pi + K \to \pi + K + \gamma$ with $K = (K^+, K^-), \pi + K^0 \to \pi + K^0 + \gamma, \pi + K^* \to \pi + K^* + \gamma$ and $\pi + K^{*0} \to \pi + K^{*0} + \gamma$. We stress again that only the elastic meson-meson collisions have been accounted here. Indeed, the final result is very sensitive to the meson-meson elastic cross section that is, however, very hard to measure experimentally. We have used a 10-mb elastic cross section for all meson-meson scatterings in the present study. As follows from Fig. 8 the dominant contribution stems from $\pi + \pi$ elastic scattering; the contributions from $\pi + K^{*0}, \pi + K^0$, and $\pi + \eta$ are also visible at low p_T. This is again consistent with Refs. [27,28] where the authors found that the photon emission rate from pion-kaon scattering is at the ~20% level of the one from pion-pion scattering.

We mention that the solid line at high p_T in Fig. 7 shows the estimated contribution from the prompt photons. For that we have convoluted the pp data fit from Ref. [44] with the nuclear overlap function T_{AB}. Indeed, it gives a lower estimate for the prompt photons because the nuclear effects (as, e.g., Cronin effect) have been ignored. For further discussions on the contributions of the prompt as well as thermal photons we refer to Refs. [26,44] and references therein.

IV. RESULTS FOR THE PHOTON PRODUCTION IN $p + A$ COLLISIONS AT SPS ENERGIES

To draw solid conclusions on the direct photons from heavy-ion collisions one needs some "reference systems," i.e., to compare to $p + p$ and/or $p + A$ data. Recently the WA98 Collaboration has provided preliminary data on $p + C$ and $p +$ Pb collisions at $\sqrt{s} = 17.4$ GeV. In this section we present the HSD results for these systems.

We start again with the inclusive invariant photon spectra from $p + C$ and $p +$ Pb collisions at midrapidity for 160A GeV that are depicted in Fig. 9. The solid dots corresponds to the preliminary WA98 data [19], the various lines stand for the HSD calculations. Again, as in a case of Pb + Pb, the dominant contribution comes from the π^0 and η photonic decays. As

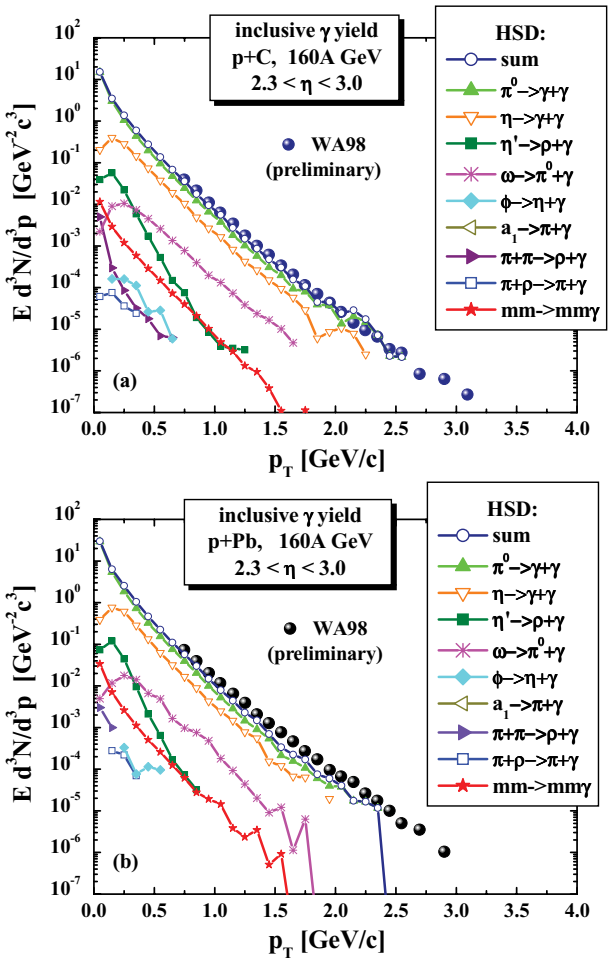

FIG. 9. (Color online) The inclusive invariant photon multiplicity for 158A GeV $p +$ ^{12}C (a) and $p +$ ^{208}Pb (b) at $2.3 \leqslant \eta \leqslant 3.0$. The solid dots corresponds to the preliminary WA98 data [19]; the lines stand for the HSD calculations. The definition of the lines is indicated in the legend.

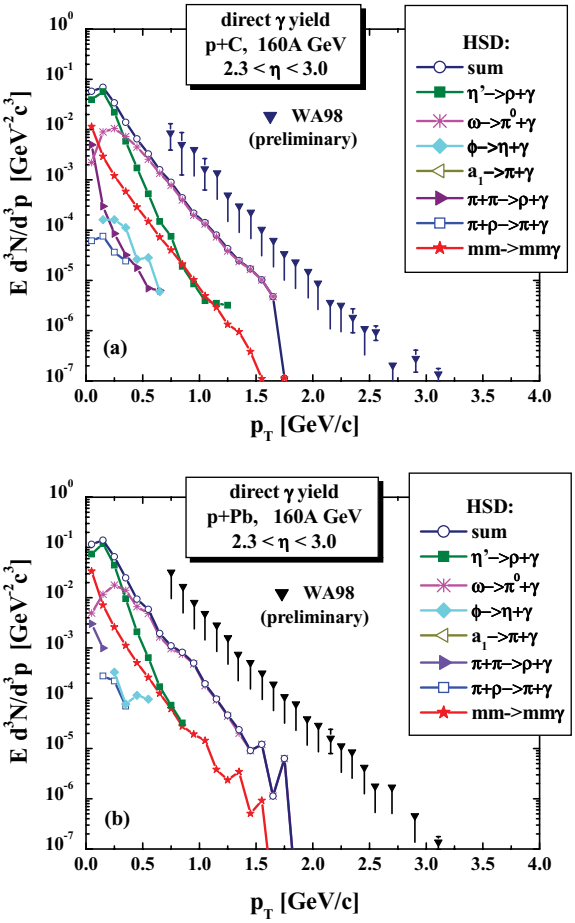

FIG. 10. (Color online) The invariant direct photon multiplicity for 158A GeV $p + {}^{12}$C (a) and $p + {}^{208}$Pb (b) at $2.3 \leqslant \eta \leqslant 3.0$. The solid dots correspond to the preliminary WA98 data [19]; the lines stand for the HSD calculations. The definition of the lines is indicated in the legend.

seen from Fig. 9 HSD provides a very good description of the inclusive experimental data.

To focus on the direct photon contribution the WA98 Collaboration has subtracted the contributions of the hadronic decays in a similar way as for the Pb + Pb collisions. However, due to experimental uncertainties in the "background" subtraction the preliminary WA98 data correspond to the upper limits on direct photon production [19] and are shown by the (down) arrows in Fig. 10 for $p + C$ (upper part) and $p +$ Pb (lower part). The various lines in Fig. 10 stand for the HSD result. Here we do not apply any cuts in density to obtain an upper estimate for the hadronic decays. Contrary to the Pb + Pb collisions the contribution from the meson-meson bremsstrahlung is suppressed compared to the η' and ω decay due to the small meson density in $p + A$ collisions. As seen from Fig. 10 the HSD results are much below the upper limits from WA98. Because it is unlikely that there are some new channels for photon production in $p + A$ reactions, which are not visible in Pb + Pb collisions, we expect that the final data might go down, too. Thus, it is quite important to obtain precise $p + A$ data from the experimental side to check the theoretical models more accurately.

V. SUMMARY

In this study a detailed analysis of the low p_T photon production in $p + C$, $p +$ Pb, and Pb + Pb collisions at 160A GeV has been presented within the microscopic HSD transport approach that incorporates a full off-shell propagation of the vector mesons [17]. We stress that the HSD approach contains only hadronic degrees of freedom and strings and does not include the phase transition from a QGP to hadronic matter explicitly; the partonic interactions are treated in HSD only inside the strings (and in terms of leading quarks and diquarks). However, the model has all nonequilibrium dynamical features and demonstrates a good ability in describing a variety observables for heavy-ion and proton- and pion- induced reactions. Accordingly, we apply our model to study the direct photon production from hadronic sources that dominate at low p_T.

In particular, the following hadronic sources for direct photon production in heavy-ion collisions have been incorporated:

(i) Photon emission from elementary meson-meson rescatterings, where the processes $\pi\rho \to \pi\gamma$ and $\pi\pi \to \rho\gamma$ are dominant due to the high pion production rate. The novel issue here is that we accounted for the off-shellness of the initial/final ρ meson and extended the vacuum cross sections for these processes from Kapusta *et al.* [29] for the in-medium case with the full off-shell ρ-meson spectral function. It allows us to investigate the influence of the in-medium effects such as "collisional broadening" on the photon p_T spectrum.

(ii) Meson-meson bremsstrahlung from the elastic meson-meson scattering $m_1 + m_2 \to m_1 + m_2 + \gamma$ (where $m = \pi, \eta, K, \bar{K}, K^0, K^*, \bar{K}^*, K^{*0}$), which we accounted for by applying the SPA formula (16).

We found that the enhancement of the low p_T photon emission from elementary meson-meson rescattering due to a collisional broadening of the vector-meson spectral functions is hardly visible in the final spectra that are dominated by bremsstrahlung-type processes. Thus our nonequilibrium dynamical calculations support the early findings in Refs. [27,28] based on the hadron gas models.

Also we have investigated the uncertainties in the extraction of the direct photon yield from the measured inclusive photon spectra that are dominated by the hadronic decays, in particular π^0, η, η', ω, and a_1. Here the HSD model shows a very good agreement with the measured inclusive photon transverse-momentum distribution. Although the background contributions from the π^0 and η decay can be subtracted in a reliable way—because these mesons are measured by the same WA98 experiment—there remains a problem in the subtraction of the contributions from short living resonances that decay inside the hot and dense fireball. We have estimated the possible contribution of such in-medium decay processes by comparing two calculations: in the first we selected the photons coming from the mesonic decays inside the fireball by applying a density cut $\rho_N \geqslant \rho_0/2$, and in the second we accounted for the mesonic decays over the full time history. We found that the density cut reduces drastically the final yield that

depends directly on the actual value of the cut. However, some amount of photons from the inside ω decay for $\rho_N \geqslant \rho_0/2$ is visible in the final spectra and might be misidentified as direct photons.

For reference we also studied the photon production for $p + C$ and $p + \mathrm{Pb}$ collisions at 160 GeV. Again, the HSD model provides a good description of the preliminary experimental data from the WA98 Collaboration on the inclusive spectra; however, is much below the upper limits for the direct photons (even without a subtraction of η', ω, ϕ, and a_1 photon decays). In this respect it will be very helpful to have the final experimental data (with high accuracy).

ACKNOWLEDGMENTS

The authors acknowledge inspiring discussions with W. Cassing, C. Gale, R. Rapp, and S. Turbide. This work was partially supported by INTAS, grant number 06-1000012-8914, and the federal agency of Russia for atomic energy (Rosatom).

[1] E. L. Feinberg, Nuovo Cimento A **34**, 391 (1976).
[2] E. Shuryak, Phys. Lett. **B78**, 150 (1978).
[3] J. D. Bjorken and H. Weisberg, Phys. Rev. D **13**, 1405 (1976).
[4] R. D. Pisarski, Phys. Rev. Lett. **63**, 1129 (1989).
[5] E. Braaten, R. D. Pisarski, and T. C. Yuan, Phys. Rev. Lett. **64**, 2242 (1990).
[6] J. Kapusta, P. Lichard, and D. Seibert, Phys. Rev. D **44**, 2774 (1991); Erratum-*ibid* **47**, 4171 (1993).
[7] D. K. Srivastava, Eur. Phys. J. C **10**, 487 (1999).
[8] Z. W. Lin *et al*., Nucl. Phys. **A698**, 375 (2002).
[9] S. A. Bass and A. Dumitru, Phys. Rev. C **61**, 064909 (2000).
[10] W. Cassing, Nucl. Phys. **A791**, 365 (2007); **A795**, 70 (2007).
[11] R. Albrecht *et al*. (WA98 Collaboration), Phys. Rev. Lett. **76**, 3506 (1996).
[12] A. Dumitru, U. Katscher, J. A. Maruhn, H. Stöcker, W. Greiner, and D. H. Rischke, Phys. Rev. C **51**, 2166 (1995).
[13] G. Q. Li, G. E. Brown, C. Gale, and C. M. Ko, nucl-th/9712048.
[14] E. L. Bratkovskaya and W. Cassing, Nucl. Phys. **A619**, 413 (1997).
[15] M. M. Aggarval *et al*. (WA98 Collaboration), nucl-ex/0006007; Phys. Rev. Lett. **85**, 3595 (2000); **93**, 022301 (2004).
[16] T. Peitzmann and M. H. Thoma, Phys. Rep. **364**, 175 (2002).
[17] E. L. Bratkovskaya and W. Cassing, Nucl. Phys. **A807**, 214 (2008).
[18] E. L. Bratkovskaya, W. Cassing, and O. Linnyk, arXiv:0805.3177 [nucl-th].
[19] C. Baumann *et al*. (WA98 Collaboration), arXiv:0804.4407 [nucl-ex].
[20] S. M. Kiselev, arXiv:hep-ph/0701130.
[21] W. Cassing and E. L. Bratkovskaya, Phys. Rep. **308**, 65 (1999).
[22] W. Ehehalt and W. Cassing, Nucl. Phys. **A602**, 449 (1996).
[23] K. Weber *et al*., Nucl. Phys. **A539**, 713 (1992).
[24] B. Anderson, G. Gustafson, and Hong Pi, Z. Phys. C **57**, 485 (1993).
[25] Particle Data Group, J. Phys. G **33**, 1 (2006).
[26] S. Turbide, R. Rapp, and C. Gale, Phys. Rev. C **69**, 014903 (2004).
[27] K. Haglin, J. Phys. G **30**, L27 (2004).
[28] W. Liu and R. Rapp, Nucl. Phys. **A96**, 101 (2007).
[29] J. Kapusta, P. Lichard, and D. Seibert, Phys. Rev. D **44**, 2774 (1991).
[30] T. Hatsuda and S. H. Lee, Phys. Rev. C **46**, R34 (1992).
[31] G. E. Brown and M. Rho, Phys. Rev. Lett. **66**, 2720 (1991).
[32] G. Chanfray, R. Rapp, and J. Wambach, Phys. Rev. Lett. **76**, 368 (1996).
[33] V. Metag, arXiv:0711.4709 [nucl-ex].
[34] K. Haglin, Nucl. Phys. **A584**, 719 (1995).
[35] D. Trnka *et al*., Phys. Rev. Lett. **94**, 192303 (2005).
[36] M. Zielinski *et al*., Phys. Rev. Lett. **52**, 1195 (1984).
[37] V. Koch, Int. J. Mod. Phys. E **6**, 203 (1997).
[38] R. Rapp, J. Phys. G **31**, S217 (2005).
[39] W. Wagner and S. Leupold, arXiv:0708.2223 [hep-ph].
[40] S. Vogel and M. Bleicher, arXiv:0710.1158 [hep-ph].
[41] C. Gale and J. Kapusta, Phys. Rev. C **35**, 2107 (1987); C. Gale and J. Kapusta, Nucl. Phys. **A495**, 423c (1989).
[42] E. L. Bratkovskaya *et al*., Phys. Rev. C **69**, 054907 (2004).
[43] W. Cassing, E. L. Bratkovskaya, and A. Sibirtsev, Nucl. Phys. **A691**, 753 (2001).
[44] D. K. Srivastava, Eur. Phys. J. C **22**, 129 (2001).